METRICA
METRology Institutional CAtalog

ISTITUTO NAZIONALE DI RICERCA METROLOGICA
Repository Istituzionale

A fully digital bridge towards the realization of the farad from the quantum Hall effect

Original
A fully digital bridge towards the realization of the farad from the quantum Hall effect / Marzano, Martina; Ortolano, Massimo; D'Elia, Vincenzo; Müller, André; Callegaro, Luca. - In: METROLOGIA. - ISSN 0026-1394. - 58:1(2021), p. 015002. [10.1088/1681-7575/abba86]

Availability:
This version is available at: 11696/64693 since: 2020-12-23T10:10:02Z

Publisher:
IOP

Published
DOI:10.1088/1681-7575/abba86

Terms of use:

This article is made available under terms and conditions as specified in the corresponding bibliographic description in the repository

Publisher copyright

(Article begins on next page)

18 December 2025

Metrologia

PAPER • OPEN ACCESS

A fully digital bridge towards the realization of the farad from the quantum Hall effect

To cite this article: Martina Marzano *et al* 2021 *Metrologia* **58** 015002

View the article online for updates and enhancements.

This content was downloaded from IP address 130.25.241.142 on 23/12/2020 at 09:04

OPEN ACCESS
IOP Publishing
Metrologia
Metrologia **58** (2021) 015002 (10pp)
https://doi.org/10.1088/1681-7575/abba86

A fully digital bridge towards the realization of the farad from the quantum Hall effect

Martina Marzano[1], **Massimo Ortolano**[1,2], **Vincenzo D'Elia**[1], **André Müller**[3] **and Luca Callegaro**[1]

[1] Istituto Nazionale di Ricerca Metrologica, Strada delle Cacce, 91, 10135 Torino, Italy
[2] Politecnico di Torino Corso Duca degli Abruzzi 24, 10129 Torino, Italy
[3] Physikalisch-Technische Bundesanstalt Bundesallee 100, 38116 Braunschweig, Germany

E-mail: m.marzano@inrim.it

Received 16 June 2020, revised 14 September 2020
Accepted for publication 22 September 2020
Published 21 December 2020

Abstract

This paper presents the implementation of an electronic fully-digital impedance bridge optimized for *RC* comparisons with equal impedance magnitudes, together with an evaluation of the uncertainty. This bridge has been designed with the goal of realizing the farad directly from the quantum Hall effect with a bridge uncertainty component at the 10^{-7} level. Thanks to its simple design, ease of operation and affordability, this bridge is suitable to be industrially manufactured. Together with the increasing availability of graphene quantum Hall resistance standards, this can provide an affordable quantum realization of the unit farad for metrology institutes and calibration centres.

In this paper we present the uncertainty budget of an example measurement and the results of the validation of the bridge against a suitably modified version of the traceability chain of the Italian national standard of capacitance. The combined uncertainty of the bridge resulted from repeated measurements (overall measurement time of about 200 min) is 9.2×10^{-8}, suitable for the primary realization of the unit of capacitance from a quantized Hall resistance standard. The crosstalk among the channels of the electrical generator is the most significant uncertainty component, possibly reducible with internal shielding and filtering of the electronic generator.

Keywords: digital impedance bridges, impedance metrology, quantum hall effect

(Some figures may appear in colour only in the online journal)

1. Introduction

In the International System of Units (SI), the units of electrical impedance ohm, henry and farad are linked by the relations $1\ \Omega = 1\ \mathrm{Hs}^{-1} = 1\ \mathrm{F}^{-1}\mathrm{s}$. Since the 2018 revision of the SI,

> The farad F can be realized […] by comparing the impedance of a known resistance obtained using the quantum Hall effect and the value of the von Klitzing constant […], including a quantized Hall resistance itself, to the impedance of an unknown capacitance using, for example, a quadrature bridge; […] [1, appendix 2]

The *quadrature bridge* mentioned in the SI brochure is a double product impedance bridge [2, 3], which compares two resistors R_1 and R_2, and two capacitors C_1 and C_2, at a properly

Original Content from this work may be used under the terms of the Creative Commons Attribution 4.0 licence. Any further distribution of this work must maintain attribution to the author(s) and the title of the work, journal citation and DOI.

 © 2020 BIPM & IOP Publishing Ltd Printed in the UK

chosen fixed angular frequency ω. The standard implementation of the quadrature bridge principle [4–8] results in a very complex electrical network with many electromagnetic components, including several multi-decade inductive voltage dividers. These variable dividers must be skilfully operated in order to achieve both the two main balances and, simultaneously, several auxiliary ones. The latter are in fact required to match the proper impedance definition of each of the four standards being compared. Automating the quadrature bridge, although possible, is cumbersome [9, 10]. Digitally-assisted implementations [11, 12] can reduce the network complexity of the quadrature bridge to some extent, and allow a partial automation. A quadrature bridge calibrates the product C_1C_2; an additional measurement with a ratio bridge is required to determine the individual values of C_1 and C_2.

The quoted SI brochure entails that R_1 and R_2 are either resistance standards having an AC value traceable to a quantized Hall resistance (QHR) standard, or that they are QHR standards themselves, measured in the AC regime (ACQHR standards). In the first case [12–14], special resistors having a calculable frequency dependence [15, 16] are calibrated in DC versus the QHR, and their values are numerically corrected. In the second case [6, 17], the effect of unwanted frequency dependencies caused by parasitic effects in the Hall device must be carefully considered [18, 19]. To date, only one laboratory worldwide operates a permanent quadrature bridge with two quantum Hall effect devices in a single cryostat [17], a massive and complex experiment filling an entire laboratory.

Fully-digital bridges [20–25] can compare a single resistor R and a single capacitor C. The fully-digital approach allows the design and implementation of much simpler bridges suitable to be industrially manufactured. Together with the increasing availability of quantum Hall graphene devices, which allow the realization of QHR standards in simpler experimental environments [26], the fully-digital approach underpins an affordable quantum realization of the unit farad by metrology institutes and calibration centres [27].

In the following, we present an electronic[4] fully-digital bridge suitable for the realization of the farad[5]. The bridge calibrates a capacitance standard of nominal value 8 nF versus a resistor R of nominal value $R_H = R_K/2 \approx 12\,906\Omega$ at the frequency[6] $f \approx 1541$ Hz.

The bridge network is very simple and is based on a multichannel polyphase electronic digital waveform generator [33]. The bridge balance is semi-automated, and the duration of an individual measurement is around 15 min. The transfer relative expanded uncertainty is about 3×10^{-7} in a single measurement (15 min) and down to 2×10^{-7} in about 5 measurements (75 min).

This work reports the principle of operation of the bridge (section 2), its implementation (section 3), a thorough analysis of the uncertainty sources (section 4), and a validation of the bridge performance, by comparison with the traceability chain of the Italian national standard of capacitance [12] (section 5).

2. Principle of operation

The *four-terminal-pair voltage-ratio fully-digital* impedance bridge described herewith is based on the principle schematic of figure 1, where the coaxial shield and terminal pairs, and a number of auxiliary components have been omitted for simplicity (the complete schematic is reported in section 3).

The driving voltages and currents E_1, E_2, E_0, E_L, I_1 and I_2 are synthesized by a polyphase digital sinusoidal waveform generator operating at frequency f and can be individually adjusted in magnitude and phase[7]. Each voltage or current corresponds to an output channel of the generator. E_1 and E_2 are the bridge main voltages; E_L, I_1 and I_2 are auxiliary voltage and currents needed to realize the impedance definition; and E_0 is an auxiliary injection voltage which, together with the injection impedance Z_0, allows to fine-tune the bridge balance.

The impedances under comparison are Z_1, with terminals HC1, HP1, LC1 and LP1, and Z_2, with terminals HC2, HP2, LC2 and LP2. In this specific application, Z_1 is the reference impedance that can be either an ACQHR standard with resistance R_H, connected with a multiple-connection scheme (see section 6), or a calibrated standard resistor with nominal resistance R_H, such that $Z_1 \approx R_H$; Z_2 is a capacitor with capacitance C, such that $Z_2 \approx 1/(\mathrm{j}2\pi fC)$; and f is chosen so that $2\pi f R_H C \approx 1$ (that is, $Z_1/Z_2 \approx \mathrm{j}$).

The bridge is balanced when $V_{LP1} = V_{LP2} = 0$ and $I_{HP1} = I_{HP2} = 0$, where the voltages V_{LP1} and V_{LP2} are measured at the impedance terminals LP1 and LP2, and the currents I_{HP1} and I_{HP2} are measured at the detection terminals DHP1 and DHP2 through the current transformers CT_1 and CT_2. The balance can be checked by cycling the synchronous detector D, referenced at the frequency f, through the detection terminals LP1, LP2, DHP1 and DHP2, and can be attained by adjusting E_2 (or E_1), E_0, E_L, I_1 and I_2 (the details of the balance procedure are discussed in section 3).

When the bridge is balanced, the impedance ratio Z_1/Z_2 is directly compared with the voltage ratio E_1/E_2, and the following balance equation holds:

$$W = \frac{Z_1}{Z_2} = -\frac{E_1}{E_2}\left(1 + \frac{E_0/Z_0}{E_1/Z_1}\right). \quad (1)$$

[4] Here, the adjective *electronic* refers to the fact that the signal generator is based on integrated electronics, in contrast with fully-digital bridges based on Josephson arbitrary waveform synthesizers [28–31].

[5] This paper is focussed on the bridge description and on its measurement capabilities; its integration with a quantum Hall effect system is under development and will be reported in a future work.

[6] The nominal values for C and f are chosen to fulfil the relationship $2\pi fRC \approx 1$. The integer value $C = 8$ nF $= 2^3$ nF allows efficient scaling to the decadal values of interest for dissemination; the frequency $f \approx 1541$ Hz is close to 1592 Hz$\approx$10 kHz/(2π), a *de facto* standard frequency for capacitance dissemination and intercomparisons [32].

[7] In the following, quantity symbols represent complex phasors associated to real voltage and current signals, or complex impedances.

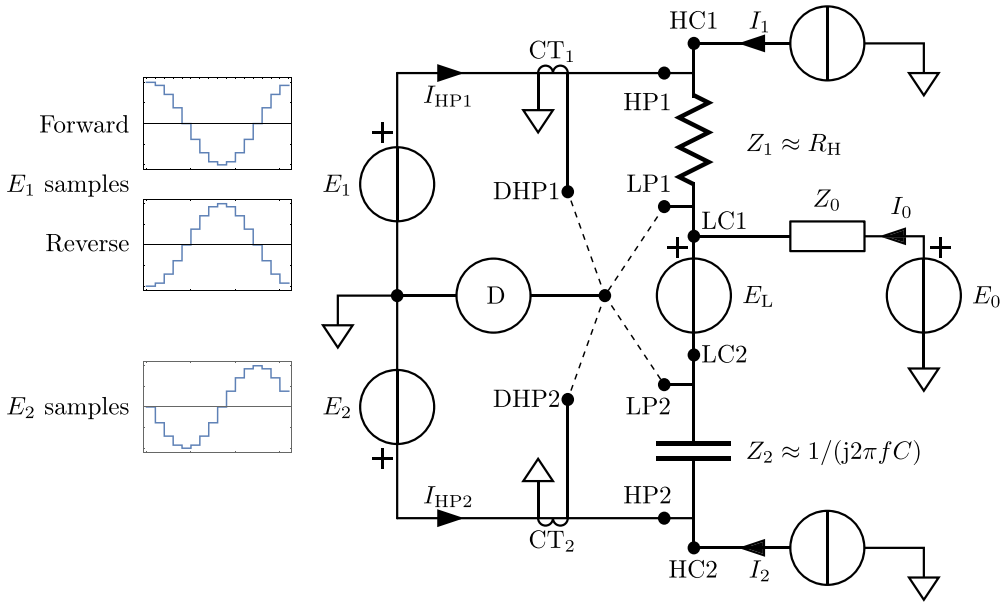

Figure 1. Simplified principle schematic of the bridge: $Z_1 \approx R_H$ and $Z_2 \approx 1/(j2\pi fC)$ are the impedances under comparison; f is the bridge operating frequency, chosen so that $2\pi f R_H C \approx 1$; E_1 and E_2 are the main bridge voltages; I_1 and I_2 are the current sources balancing I_{HP1} and I_{HP2}; E_L is the voltage source balancing the difference $V_{LP1} - V_{LP2}$; CT1 and CT2 are current transformers measuring the currents I_{HP1} and I_{HP2}, respectively; the voltage source E_0 and the impedance Z_0 constitute an auxiliary injection arm to fine-tune the bridge balance; and D is a synchronous detector that can be connected, in turn, to the detection terminals LP1, LP2, DHP1 and DHP2. The diagrams on the left represent example waveform samples: the samples of E_1 are changed in sign between the forward and reverse configurations; the samples of E_2 are instead kept fixed.

Alternatively, by considering the admittances $Y_1 = 1/Z_1$, $Y_2 = 1/Z_2$ and $Y_0 = 1/Z_0$,

$$W = \frac{Y_2}{Y_1} = -\frac{E_1}{E_2}\left(1 + \frac{E_0 Y_0}{E_1 Y_1}\right). \tag{2}$$

As can be seen from the above equations, by choosing $|Z_0| \gg |Z_1|$, the voltage E_0 can be used to fine-tune the bridge balance around the ratio $-E_1/E_2$. This is instrumental to achieve the highest measurement accuracy, as described below.

The voltage phasors E_1 and E_2 can be computed from the samples used to synthesize the two waveforms. We take the readings E_1^{read} and E_2^{read} from the fundamental components at frequency f of the Fourier series representing the waveform samples. Due to the generator non-idealities, the actual voltages will differ from the readings and we can write $E_k = [1 + g_k(E_k^{\text{read}})]E_k^{\text{read}}$, $k = 1, 2$, with $g_k(E_k^{\text{read}})$ representing a possibly voltage-dependent complex gain error (for magnitude and phase errors), thus considering a possible generator non-linearity. This is actually the main source of error in fully-digital bridges [23, 34].

The error described above can be perfectly cancelled by performing two measurements: one with the impedances connected as in figure 1 (*forward* configuration) and one with the two impedances exchanged (*reverse* configuration), and by imposing that the samples used to generate E_1 and E_2 are *exactly* the same in the two configurations, at most shifted in time, as shown on the left of figure 1 (how this condition can be imposed is described in section 3). This is feasible because with the conditions introduced at the beginning of this section, the magnitude of the impedance ratio is about 1 in both the forward and reverse configurations, $|Z_2/Z_1| \approx |Z_1/Z_2| \approx 1$, and its phase changes by about 180° because $\arg(Z_2/Z_1) = -\arg(Z_1/Z_2) \approx 90°$. Therefore, to balance the reverse configuration, we just need to change the sign of all the samples of either E_1 or E_2 (equivalent to a 180° shift), and re-adjust the injection voltage E_0.

For the forward (F subscript) and reverse (R subscript) configurations, the balance equations are

$$W = W_F = -\frac{E_{1F}}{E_{2F}}\left(1 + \frac{E_{0F} Y_0}{E_{1F} Y_1}\right), \tag{3}$$

$$W = W_R = -\frac{E_{2R}}{E_{1R}}\left(1 + \frac{E_{0R} Y_0}{E_{2R} Y_1}\right), \tag{4}$$

from which

$$W = \sqrt{W_F W_R}, \tag{5}$$

where the complex square root in (5) should be determined with a positive imaginary part because $W \approx \mathrm{j}$.

According to the foregoing argument, $E_{1R}/E_{2R} = -E_{1F}/E_{2F}$, *exactly*, by construction of the waveform samples, such that, from (3)–(5),

$$W = \mathrm{j}\sqrt{\left(1 + \frac{E_{0F} Y_0}{E_{1F} Y_1}\right)\left(1 + \frac{E_{0R} Y_0}{E_{2R} Y_1}\right)}, \tag{6}$$

thus cancelling any major error due to $g_k(E_k^{\text{read}})$ (minor errors are discussed in section 4).

From W and the reference impedance Z_1, the capacitance C can be finally determined as

$$C = \frac{1}{2\pi f}\mathrm{Im}\frac{W}{Z_1} = \frac{1}{2\pi f}\mathrm{Im}(WY_1), \tag{7}$$

where Im denotes the imaginary part of its argument.

3. Bridge implementation

Figures 2 and 3 show the coaxial schematic and a photograph of the bridge.

This section describes only the implementation of the bridge network; the impedances Z_1 and Z_2 employed in the validation are described in section 5.

At the core of the bridge there is the adjustable polyphase digital sinusoidal waveform generator described in [35][8]. This digital signal source is based on 18 bit digital-to-analogue converters with adjustable range (1 V, 2.5 V, 5 V and 10 V) and isolated precision filter/buffer output stages [37]. The relative amplitude and phase stability of the source are about $10^{-7}\mathrm{h}^{-1}$. A National Instruments NI-DAQ 6541 board generates the digital codes of the waveform samples, which are then transmitted to the source. The waveform is composed of a fixed integer number of samples per period[9] and the frequency is adjusted through the sample rate and the number of samples. This yields the possibility to control the output samples and obtain a simple and computable output spectrum. A channel reading is then obtained from the latter. The clock of the digital source, which defines the sample rate, is locked to a 10 MHz signal from the Italian national time scale.

The digital source provides seven independent output channels, necessary for the complete implementation of the bridge. Two channels generate the voltages E_1 and E_2, which provide the voltage ratio reference against which the impedance ratio is compared. The $R_{S1} = R_{S2} = 10\ \Omega$ resistors (Vishay S102 series), in series to E_1 and E_2, isolate the channel outputs from the capacitive load, avoiding possible self-oscillations of the output buffers.

Three channels generate the voltages E_3, E_4 and E_L which drive the auxiliary circuits realizing the four terminal-pair impedance definition. The currents I_1 and I_2 are generated by E_3 and E_4 through the $R_{S3} = R_{S4} = 100\ \Omega$ resistors (Vishay S102 series). Two dummy loads $C_L \approx C$ and $R_L \approx R_H$ are added at the HC ports of the impedances to symmetrize the source loading in both forward and reverse configurations.

One channel generates the voltage E_L through a 200 : 1 feedthrough injection voltage transformer. One channel generates the voltage E_0 which provides the auxiliary injection through the $C_0 = 1$ pF capacitor, which corresponds to Z_0 in figure 1. One further channel generates the reference signal for the phase-sensitive detector.

The phase-sensitive detector is a Stanford Research SR830 lock-in amplifier and is used to detect the bridge balance on the fundamental component of the signal.

The detector is manually switched across the positions V_{DHP1} and V_{DHP2}, measuring the currents I_{HP1} and I_{HP2} through the 1:200 feedthrough transformers CT_1 and CT_2, and the positions V_{LP1} and V_{LP2}.

Both the digital source and the detector are controlled by a software purposely coded in the National Instruments LabWindows/CVI environment and based on the balancing algorithm presented in [39]. The bridge balance procedure is thus semi-automated and a single complete measurement (forward/reverse) requires about 15 min. According to what was introduced in section 2, when switching between the forward and reverse configurations, we can change the phase of E_1 by 180° and keep E_2 fixed. The digital source employed in this implementation allows to read the generated samples verifying that they are exactly matched with a 180° phase shift.

Before beginning a series of measurements, it is convenient to preset the main voltages E_1 and E_2 to minimize the auxiliary injection E_0. Starting from the set-up shown in figure 2, the preliminary procedure can be done in the following way:

P1. Set E_0 to 0 V, and E_1 to the operating value of interest.
P2. Short circuit both V_{LP1} and V_{LP2}.
P3. Adjust E_3 to null the detector connected to V_{DHP1}.
P4. Adjust E_4 to null the detector connected to V_{DHP2}.
P5. Remove the short circuit at V_{LP1}.
P6. Adjust E_5 to null the detector connected to V_{LP1} (this actually nulls the differential voltage $V_{LP1} - V_{LP2}$).
P7. Remove the remaining short circuit at V_{LP2}.
P8. Adjust E_2 to null the detector connected to V_{LP1}.
P9. Adjust E_4 to null the detector connected to V_{DHP2}.
P10. Repeat steps P8 and P9 until the detector is nulled simultaneously within the chosen thresholds for both detection ports.
P11. Record the voltage reading E_{2F}^{read} for the forward configuration.
P12. Change set-up from the forward configuration to the reverse one by swapping the cables between $E_1 \leftrightarrow E_2$ and $E_3 \leftrightarrow E_4$, and by shifting the phase of E_1 by 180°.
P13. Repeat steps P1 through P10 and record the voltage reading E_{2R}^{read} for the reverse configuration.
P14. Set E_2 in both configurations to the geometric mean $E_2 = \sqrt{E_{2F}^{read}E_{2R}^{read}}$.

The measurement procedure is then as follows:

M1. In the forward configuration, execute the steps P2 through P7 of the preliminary procedure and finally adjust E_0 to null the detector connected to V_{LP1}. Record the readings E_{0F}^{read}, E_{1F}^{read} and E_{2F}^{read}.
M2. In the reverse configuration, execute the steps P2 through P7 of the preliminary procedure and finally adjust E_0 to null the detector connected to V_{LP1}. Record the readings E_{0R}^{read}, E_{1R}^{read} and E_{2R}^{read}.
M3. Calculate W from (19), section 4.5.

[8] The generator was developed by Janusz Kaczmarek and Ryszard Rybski, University of Zielona Góra (UZG), Poland, in the framework of the European project EMRP SIB53 AIM QuTE: *Automated impedance metrology extending the quantum toolbox for electricity* [36].

[9] Unlike what happens in a direct-digital synthesizer (DDS) with phase accumulation [38].

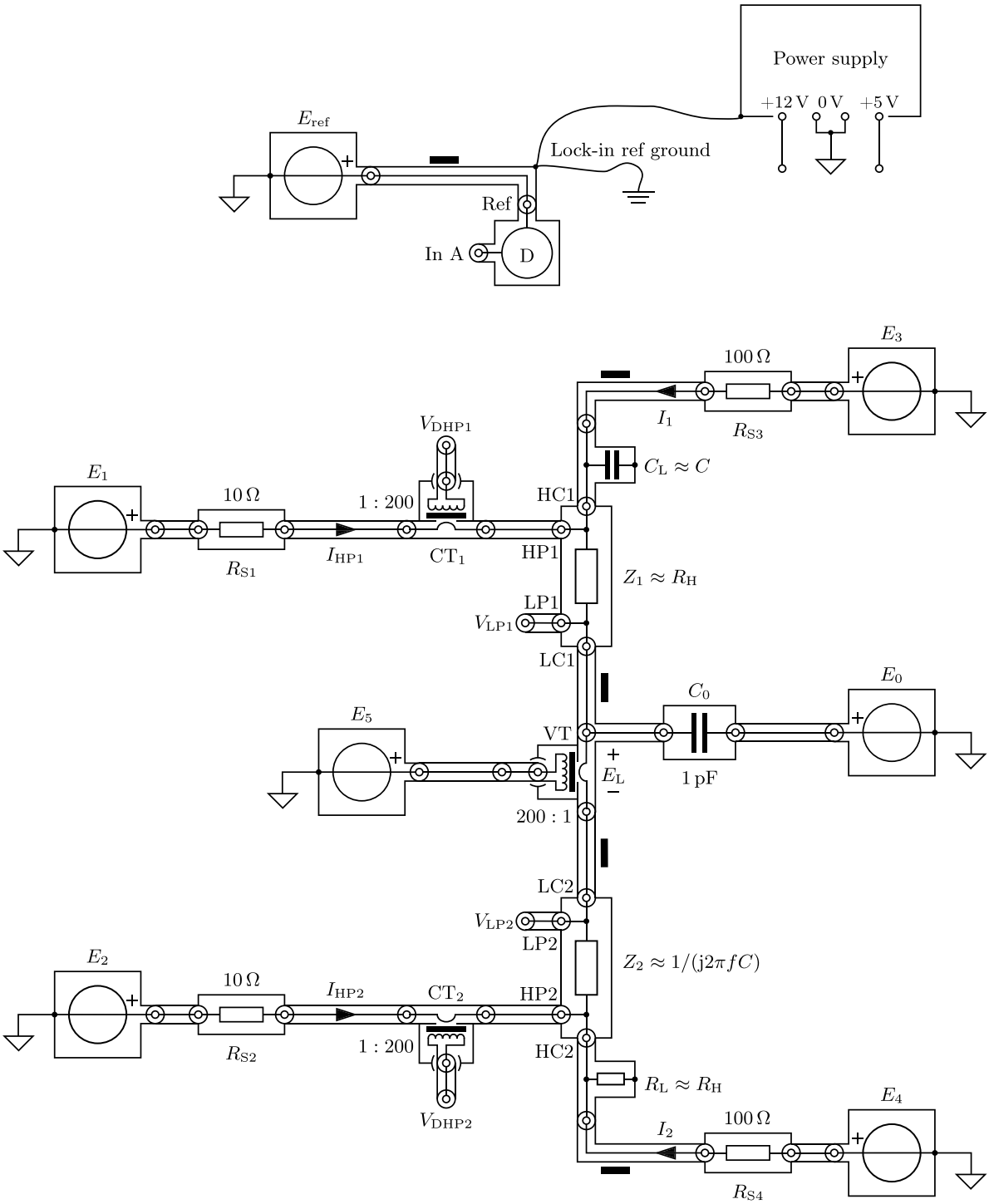

Figure 2. Coaxial implementation of the principle schematic diagram of figure 1. Injection/detection transformers provide the voltage E_{L} and the detection of V_{DHP1} and V_{DHP2}. Each black rectangle represents a coaxial equalizer.

M4. The capacitance C is determined, from W and the impedance Z_1, as in (7).

We note the following: i) even though the bridge balance procedure can be completely automated with an external switch, we preferred the semi-automated approach to avoid the risk of worsening the crosstalk between the source channels (see section 4.2); and ii) the steps P5 and P6 of the preliminary procedure can be substituted with a measurement with the detector set in the differential input configuration.

4. Uncertainty sources and budget

This section presents an evaluation of the uncertainty for the ratio $W = Z_1/Z_2$ as defined by (5). The uncertainty sources are first described separately and then the relevant ones are combined in a measurement model which is used in reporting the uncertainty budget (for a review on the error sources in digital impedance bridges see also [34]).

In the following, according to the notation introduced in section 2, the subscripts 'F' and 'R' designate quantity values obtained in the forward and reverse configurations, respectively; the superscript 'read' designates quantity values read off the generator settings, as described in section 1. From (3)–(5) we also define

$$W_{\mathrm{F}}^{\mathrm{read}} = -\frac{E_{1\mathrm{F}}^{\mathrm{read}}}{E_{2\mathrm{F}}^{\mathrm{read}}}\left(1+\frac{E_{0\mathrm{F}}^{\mathrm{read}}Y_0}{E_{1\mathrm{F}}^{\mathrm{read}}Y_1}\right), \tag{8}$$

$$W_{\mathrm{R}}^{\mathrm{read}} = -\frac{E_{2\mathrm{R}}^{\mathrm{read}}}{E_{1\mathrm{R}}^{\mathrm{read}}}\left(1+\frac{E_{0\mathrm{R}}^{\mathrm{read}}Y_0}{E_{2\mathrm{R}}^{\mathrm{read}}Y_1}\right) \tag{9}$$

and

$$W^{\mathrm{read}} = \sqrt{W_{\mathrm{F}}^{\mathrm{read}}W_{\mathrm{R}}^{\mathrm{read}}}. \tag{10}$$

4.1. Type A uncertainty

In this experiment, the type A uncertainty mainly depends on the noise at the detection ports LP1, LP2, DHP1 and DHP2, on the mutual impedance Z_{m} of the current transformers CT1 and CT2, on the detector time constants and thresholds chosen to stop the bridge balancing at the various detection ports, and on the instabilities of the source and the standards.

The contribution of the low balance to the type A uncertainty component of W, for a single measurement, should be expected of the order of $|\delta V_{\mathrm{L}}/E_{1,2}|$, δV_{L} being the spread of the residual voltages at LP1 and LP2. The contribution of the high balance should be expected of the order of $|R_{\mathrm{s1,s2}}\,\delta V_{\mathrm{H}}/(Z_{\mathrm{m}}E_{1,2})|$, δV_{H} being the spread of the residual voltages at DHP1 and DHP2 (see [34] for a more detailed analysis).

For the current setup we set the thresholds for the balances at LP1 and LP2 to 30 nV (1 s detector time constant) and the thresholds for the balances at DHP1 and DHP2 to 200 nV (300 ms detector time constant). With these settings, taking into account that $|Z_{\mathrm{m}}| \approx 240\ \Omega$, the projected type A uncertainty component is about 10^{-7} for a single measurement.

4.2. Crosstalk

Crosstalk is the phenomenon by which the voltage at one channel of the polyphase generator is coupled to that of another channel. Considering just the channels that may induce significant variations when switching between the forward and reverse configurations, and that $E_3 \approx E_1$ and $E_4 \approx E_2$, we can therefore write

$$E_1 = E_1^{\mathrm{read}} + E_{10} + a_{12}E_2^{\mathrm{read}} + a_{10}E_0^{\mathrm{read}}, \tag{11}$$

$$E_2 = E_2^{\mathrm{read}} + E_{20} + a_{21}E_1^{\mathrm{read}} + a_{20}E_0^{\mathrm{read}}. \tag{12}$$

In the above equations, E_{10} and E_{20} represent possible residual voltages at the source outputs, independent of $E_0^{\mathrm{read}}, E_1^{\mathrm{read}}$ and E_2^{read}, and which can be due to the crosstalk from E_{ref} or a clock feedthrough; and a_{ij} is the (complex) coupling coefficient from channel j to channel i.

Due to crosstalk, the equality $E_{1\mathrm{R}}/E_{2\mathrm{R}} = -E_{1\mathrm{F}}/E_{2\mathrm{F}}$, obtained in section 1 from the construction of the samples, no longer holds exactly. As a consequence, an error arises. By combining (11) and (12) with (3)–(5), and simplifying, we obtain at first order in the coupling coefficients

$$W = W^{\mathrm{read}} - \Delta W^{\mathrm{CT}} \tag{13}$$

with the error ΔW^{CT} given by

$$\begin{aligned}\frac{\Delta W^{\mathrm{CT}}}{W^{\mathrm{read}}} \approx -\frac{1}{2}\Bigg[&E_{10}\left(\frac{1}{E_{1\mathrm{F}}^{\mathrm{read}}}-\frac{1}{E_{1\mathrm{R}}^{\mathrm{read}}}\right)\\ &-E_{20}\left(\frac{1}{E_{2\mathrm{F}}^{\mathrm{read}}}-\frac{1}{E_{2\mathrm{R}}^{\mathrm{read}}}\right)+a_{12}\left(\frac{E_{2\mathrm{F}}^{\mathrm{read}}}{E_{1\mathrm{F}}^{\mathrm{read}}}-\frac{E_{2\mathrm{R}}^{\mathrm{read}}}{E_{1\mathrm{R}}^{\mathrm{read}}}\right)\\ &-a_{21}\left(\frac{E_{1\mathrm{F}}^{\mathrm{read}}}{E_{2\mathrm{F}}^{\mathrm{read}}}-\frac{E_{1\mathrm{R}}^{\mathrm{read}}}{E_{2\mathrm{R}}^{\mathrm{read}}}\right)+a_{10}\left(\frac{E_{0\mathrm{F}}^{\mathrm{read}}}{E_{1\mathrm{F}}^{\mathrm{read}}}-\frac{E_{0\mathrm{R}}^{\mathrm{read}}}{E_{1\mathrm{R}}^{\mathrm{read}}}\right)\\ &-a_{20}\left(\frac{E_{0\mathrm{F}}^{\mathrm{read}}}{E_{2\mathrm{F}}^{\mathrm{read}}}-\frac{E_{0\mathrm{R}}^{\mathrm{read}}}{E_{2\mathrm{R}}^{\mathrm{read}}}\right)\Bigg].\end{aligned} \tag{14}$$

The measured average magnitudes of E_{10} and E_{20} are of the order 30 nV, with a high phase uncertainty. For a reasonably conservative evaluation of the uncertainty, for E_{10} and E_{20}, we assumed uncorrelated real and imaginary parts centred around 0 with a standard uncertainty of 30 nV for each part, corresponding to a square coverage region. The measured magnitudes of the coupling coefficients between the different channels of the polyphase generator are less than 2×10^{-8}, with a high phase uncertainty. For these coefficients, we assumed uncorrelated real and imaginary parts centred around 0 with a standard uncertainty of 2×10^{-8} for each part.

4.3. Injection uncertainty

The injection terms in (3) and (4) depend on the voltage ratios $E_{0\mathrm{F}}/E_{1\mathrm{F}}$, $E_{0\mathrm{R}}/E_{2\mathrm{R}}$ and on the admittances Y_0 and Y_1. The voltage ratios can be written as

$$\frac{E_{0\mathrm{F}}}{E_{1\mathrm{F}}} = (1+g_{01})\frac{E_{0\mathrm{F}}^{\mathrm{read}}}{E_{1\mathrm{F}}^{\mathrm{read}}} \tag{15}$$

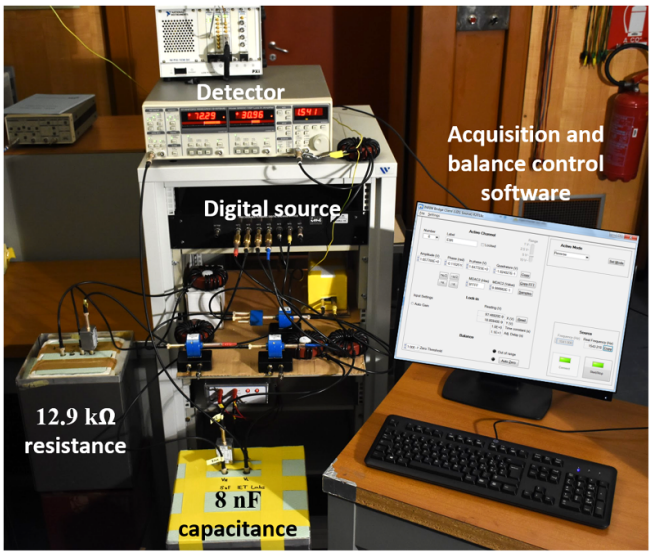

Figure 3. Picture of the experimental set-up.

and

$$\frac{E_{0R}}{E_{2R}} = (1+g_{02})\frac{E_{0R}^{\text{read}}}{E_{2R}^{\text{read}}} \tag{16}$$

where the complex error terms g_{01} and g_{02} account for the generator non-linearity as described in section 1.

A characterization of the source yielded for $1+g_{01}$ and $1+g_{02}$ a magnitude uncertainty of about 10^{-4} and an angle uncertainty of about 10^{-4} rad. The uncertainty contributions of Y_0 and Y_1 are typically negligible.

4.4. Source loading

When the bridge is balanced, the currents crossing CT1 and CT2 are approximately zero, but E_1 and E_2 are still loaded by the stray capacitances C_{H1} and C_{H2} of the cables connecting the channels to the current transformers.

When reversing the channels at the source ports, as is done in this experiment, this causes an error such that [23, 34]

$$W \approx W^{\text{read}}\left[1-\tfrac{1}{2}(R_{s1}+R_{s2})(Y_{H1}-Y_{H2})\right] \tag{17}$$

$$\approx W^{\text{read}}\left[1-\mathrm{j}\pi f(R_{s1}+R_{s2})(C_{H1}-C_{H2})\right], \tag{18}$$

where Y_{H1} and Y_{H2} are the admittances of C_{H1} and C_{H2}, respectively. If the bridge construction is symmetric, the difference $C_{H1}-C_{H2}$ is small. Since $W^{\text{read}} \approx \mathrm{j}$, the expression in the brackets changes at first order only the real part of W^{read} and not its imaginary part. Therefore, from (7), the resulting error on C is negligible at the target uncertainty level of this experiment and will not be considered in the measurement model of the next section.

Table 1. Example uncertainty budget for $\Delta = \mathrm{Im}W - 1$. All the uncertainties are standard uncertainties ($k=1$).

i	Quantity	Type	$u_i(\Delta)\times 10^6$
1	Bridge reading ($n=13$)	A	0.022
2	Crosstalk (ΔW^{CT})	B	0.089
5	Injection	B	0.01
		RSS	0.092

4.5. Measurement model and uncertainty budget

By combining the above results with (6), we obtain the measurement model

$$W = \mathrm{j}\sqrt{\left[1+(1+g_{01})\frac{E_{0F}^{\text{read}}Y_0}{E_{1F}^{\text{read}}Y_1}\right]\left[1+(1+g_{02})\frac{E_{0R}^{\text{read}}Y_0}{E_{2R}^{\text{read}}Y_1}\right]} - \Delta W^{\text{CT}}. \tag{19}$$

Table 1 reports the uncertainty budget of an example measurement for the quantity $\Delta = \mathrm{Im}W - 1$ (because $W \approx \mathrm{j}$). All the uncertainties are standard uncertainties ($k=1$). The measurement was performed on 20 February 2020 and it is also discussed in section 5.1. The driving rms voltages $|E_{1,2}| \approx 0.25$ V are chosen so that the driving current $I \approx 20$ µA flowing in the standards is suitable for the QHR. We performed the propagation of uncertainty according to [40] with the help of `Metas.UncLib` [41].

The measurement consisted in $n=13$ repetitions of forward and reverse measurements, for an overall measurement time of about 200 min and a type A uncertainty component of 2.2×10^{-8}, in reasonable agreement with the value obtainable from the projection of section 4.1 ($\approx \times 10^{-7}/\sqrt{13}$). The most significant uncertainty component is that associated to ΔW^{CT}, which was evaluated from (14) and the measurements of the coupling coefficients.

The combined uncertainty is $u_c(\Delta) \approx 9.2\times 10^{-8}$, which is competitive for the primary realization of the unit of capacitance. Since the type A uncertainty is much smaller than the type B, 5 measurements are enough to reach a combined uncertainty of 2×10^{-7}.

5. Validation

The validation of the bridge performance was obtained by comparing the 8 nF capacitor calibration performed with the four-terminal-pair fully-digital bridge with that performed with the traceability chain of the Italian national standard of capacitance [12]. The latter is typically employed to calibrate a 1 nF capacitance standard against a calibrated 12 906 Ω quadrifilar resistance standard, but it is here adapted to calibrate the 8 nF capacitance standard.

Figure 4 shows the measurement chain adopted in the validation process.

On one side of the chain, two resistance standards R_1 and R_2 of nominal value $R_{1,2} \approx 8R_H \approx 103.251$ kΩ are calibrated with a 8:1 transformer-ratio resistance bridge against a resistance standard of nominal value $R_H = R_K/2 \approx 12\,906$ Ω.

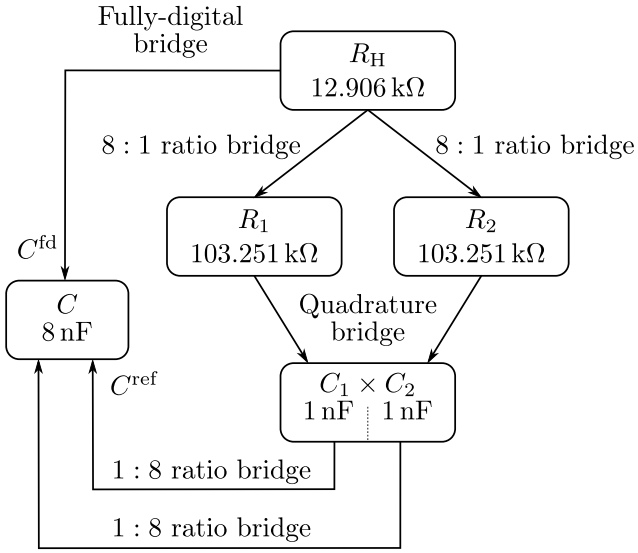

Figure 4. Diagram of the procedure adopted to compare the calibration of the 8 nF capacitance standard performed with the four-terminal-pair fully-digital bridge and that performed with the traceability chain of the Italian national standard of capacitance.

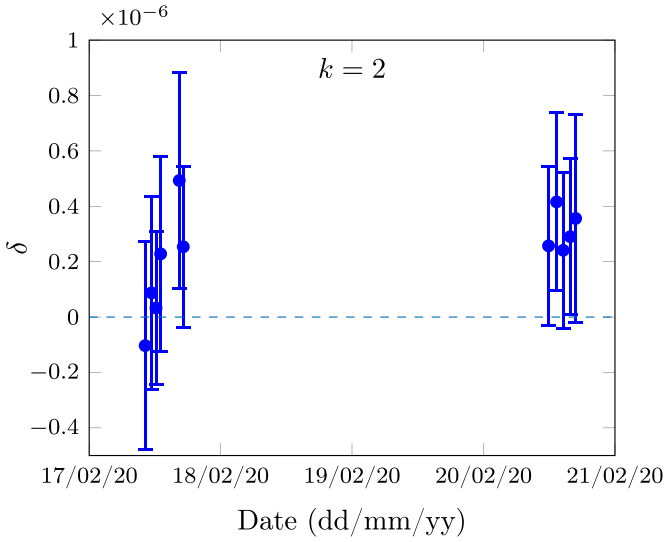

Figure 5. Comparison between the calibrations of an 8 nF capacitance standard performed with the four-terminal-pair fully-digital bridge described in the paper and with the Italian capacitance traceability chain, suitably modified. The plot represents the quantity $\delta = (C^{fd} - C^{ref})/C^{ref}$.

These resistance standards are then employed in a transformer-ratio quadrature bridge to calibrate the product C_1C_2 of two 1 nF capacitance standards. By means of a double calibration of the 8 nF capacitance standard against C_1 and C_2 with a 1:8 transformer-ratio bridge, C^{ref} is then obtained from the product C_1C_2.

On the other side, the calibration C^{fd} of the 8 nF is performed with the four-terminal-pair fully-digital bridge against the same 12 906 Ω resistance standard employed before, as described in section 3.

The two calibrations are performed at the same operating frequency of 1541.4326 978 Hz and current of 20 μA. This frequency is chosen to minimize the injections of both the fully-digital bridge and the quadrature bridge. For the fully-digital bridge, the residual deviation from the optimum condition $W = \mathrm{j}$ is about 3.5×10^{-5}.

During the measurement procedure, the 8 nF capacitance standard is kept in a temperature-controlled chamber (Kambič TK-190 US) with a temperature stability better than 4 mK [42]. Since the temperature coefficient of the capacitance standard is $4 \pm 6 \times 10^{-6}$ °C^{-1} [43], the maximum effect due to the temperature dependence is about 4×10^{-8} and can be considered virtually negligible with respect to the other uncertainty components. However, even though hermetically sealed in dry nitrogen, the 8 nF capacitance standard shows a significant dependence on the atmospheric pressure [44], evaluated in section 5.1.

5.1. Results

The result of the comparison is the relative difference

$$\delta = \frac{C^{fd} - C^{ref}}{C^{ref}}. \tag{20}$$

Figure 5 reports the results of the comparisons performed on 17 and 20 February 2020. Each point in the plot represents the result of the comparison of the average of two successive measurements of C^{fd} with one measurement of C^{ref}.

For the setup of 17 February, the thresholds were set to 50 nV for the balances at LP1 and LP2 and to 500 nV for the balances at DHP1 and DHP2. For the setup of 20 February, the thresholds were set to 30 nV for the balances at LP1 and LP2 and to 200 nV for the balances at DHP1 and DHP2. The latter set of parameters lead to an improved repeatability and it will be therefore considered an optimal trade-off between repeatability and balancing time.

The dependence on the atmospheric pressure of the 8 nF capacitance standard, introduced in section 5, is checked at regular time intervals with an ultra-precision capacitance bridge (Andeen-Hagerling 2700A). The instability component of the capacitance standard is thus considered for each measurement in the uncertainty of δ, which is calculated by combining the uncertainties of C^{fd} and C^{ref}. The expanded uncertainty of C^{ref} is $U(C^{ref}) \approx 2 \times 10^{-7}$, higher than the one stated in [12] to take into account the adaptation of the measuring chain.

In figure 5, the uncertainty bars represent the expanded uncertainties with coverage factor $k = 2$.

For the measurements of 20 February, the mean value is $\delta \approx 3.0 \times 10^{-7}$ with an expanded uncertainty $U(\delta) \approx 2.9 \times 10^{-7}$.

6. Conclusions and outlook

We presented the design, the implementation and the uncertainty evaluation of a four-terminal-pair fully-digital impedance bridge, optimized for *RC* comparisons with 1:1

magnitude ratio. Here the bridge was applied to compare a resistance standard with nominal value of R_H with an 8 nF capacitance standard at 1541 Hz (a 10 nF standard capacitor can be for instance measured at 1233 Hz). We reported the uncertainty budget of an example measurement consisted in 13 repetitions of forward and reverse measurements (overall measurement time of about 200 min). The type A uncertainty component is of 2.2×10^{-8}, while the most significant uncertainty component is that associated to the crosstalk among the channels of the generator, which is about 8.9×10^{-8}. The combined uncertainty is 9.2×10^{-8}, suitable for the primary realization of the unit of capacitance from a QHR standard. It should be noted that, since the type A uncertainty component is much less than the type B component, 5 measurements (overall measurement time of about 75 min) are enough to reach a combined expanded uncertainty of 2×10^{-7}. The bridge was validated against a suitably modified version of the traceability chain of the Italian national standard of capacitance.

This bridge is intended to be a much simpler, easy-to-operate and affordable alternative to traditional bridges, suitable to be industrially manufactured. Together with the increasing availability of graphene quantum Hall resistance standards, this can provide an affordable quantum realization of the unit farad for metrology institutes and calibration centres. The accuracy can be further improved by means of internal shielding and filtering of the generator to reduce the crosstalk among the channels.

To employ this bridge with a QHR standard it is necessary to adopt a multiple-connection scheme [45] and possibly a double-shield technique [46]. The integration of the bridge with a QHR standard will be the subject of a future work.

Acknowledgment

This project (18SIB07 GIQS) received funding from the European Metrology Programme for Innovation and Research (EMPIR) co-financed by the Participating States and from the European Unions' Horizon 2020 research and innovation programme.

ORCID iDs

Martina Marzano https://orcid.org/0000-0001-5288-3093
Massimo Ortolano https://orcid.org/0000-0002-7217-8276
Vincenzo D'Elia https://orcid.org/0000-0001-6924-0430
Luca Callegaro https://orcid.org/0000-0001-5997-9960

References

[1] Bureau International des Poids et Mesures 2019 SI brochure 9th edn [Online] Available: (https://www.bipm.org/utils/common/pdf/si-brochure/SI-Brochure-9-EN.pdf)

[2] Millea A and Ilie P 1969 A class of double-balance quadrature bridges for the intercomparison of three-terminal resistance, inductance and capacitance standards *Metrologia* **5** 14

[3] Callegaro L 2013 *Electrical Impedance: Principles, Measurement and Applications* Series in Sensors (Boca Raton, FL: CRC Press)

[4] Hsu J C and Ku Y-S 2000 Comparison of capacitance with resistance by IVD-based quadrature bridge at frequencies from 50 Hz to 10 kHz *Conf. on Precision Electromagnetic Measurements (CPEM 2000)* (Sydney, Australia, 14-19 May) pp 429–30

[5] Awan S, Kibble B and Schurr J 2011 *Coaxial Electrical Circuits for Interference-Free Measurements* Electrical Measurement Series (London: The Institution of Engineering and Technology)

[6] Chua S W, Kibble B P and Hartland A 1999 Comparison of capacitance with ac quantized Hall resistance *IEEE Trans. Instr. Meas.* **48** 342–5

[7] Small G W, Fiander J R and Coogan P C 2001 A bridge for the comparison of resistance with capacitance at frequencies from 200 Hz to 2 kHz *Metrologia* **38** 363

[8] Boháček J 2001 A multifrequency quadrature bridge *IMTC 2001. Proc. of the 18th IEEE Instrumentation and Measurement Conf.* (Budapest, Hungary, 21–23 May) vol 1 pp 102–5

[9] PTB, NPL, IEN, METAS, CTU, NML and INETI 2001 modular system for the calibration of capacitance standards based on the quantum Hall effect *Documentation and operating manual* Eur. Project SMT4–CT98–2231 Final Rep.

[10] Melcher J *et al* 2003 The European ACQHE project: modular system for the calibration of capacitance standards based on the quantum Hall effect *IEEE Trans. Instrum. Meas.* **52** 563–8

[11] Trinchera B, Callegaro L and D'Elia V 2009 Quadrature bridge for *R-C* comparisons based on polyphase digital synthesis *IEEE Trans. Instrum. Meas.* **58** 202–6

[12] Callegaro L, D'Elia V and Trinchera B 2010 Realization of the farad from the dc quantum Hall effect with digitally assisted impedance bridges *Metrologia* **47** 464

[13] Jeffery A, Elmquist R E, Shields J Q, Lee L H, Cage M E, Shields S H and Dziuba R F 1998 Determination of the von Klitzing constant and the fine-structure constant through a comparison of the quantized Hall resistance and the ohm derived from the NIST calculable capacitor *Metrologia* **35** 83

[14] Awan S A, Jones R G and Kibble B P 2003 Evaluation of coaxial bridge systems for accurate determination of the SI farad from the DC quantum hall effect *Metrologia* **40** 264

[15] Gibbings D L H 1963 A design for resistors of calculable a.c./d.c. resistance ratio *Proc. Inst. Elec. Eng.* **110** 335–47

[16] Haddad R J 1969 A Resistor Calculable From DC to $\omega = 10^5$ rad/s *MS Thesis* Sch. Eng. Appl. Sci, George Washington University

[17] Schurr J, Bürkel V and Kibble B P 2009 Realizing the farad from two ac quantum Hall resistances *Metrologia* **46** 619

[18] Schurr J, Ahlers F J, Hein G and Pierz K 2006 The ac quantum Hall effect as a primary standard of impedance *Metrologia* **44** 15

[19] Schurr J, Kučera J, Pierz K and Kibble B P 2011 The quantum Hall impedance standard *Metrologia* **48** 47

[20] Bachmair H and Vollmert R 1980 Comparison of admittances by means of a digital double-sinewave generator *IEEE Trans. Instrum. Meas.* **29** 370–2

[21] Ramm G and Moser H 2003 Calibration of electronic capacitance and dissipation factor bridges *IEEE Trans. Instrum. Meas.* **52** 396–9

[22] Lan J, Zhang Z, Li Z, He Q, Zhao J and Lu Z 2012 A digital compensation bridge for *R-C* comparisons *Metrologia* **49** 266

[23] Callegaro L, D'Elia V, Kampik M, Kim D B, Ortolano M and Pourdanesh F 2015 Experiences with a two-terminal-pair digital impedance bridge *IEEE Trans. Instrum. Meas.* **64** 1460–5

[24] Kürten Ihlenfeld W G and de Barros e Vasconcellos R T 2017 A digital five-terminal impedance bridge *IEEE Trans. Instrum. Meas.* **66** 1546–52

[25] Kučera J and Kováč J 2018 A reconfigurable four terminal-pair digitally assisted and fully digital impedance ratio bridge *IEEE Trans. Instrum. Meas.* **67** 1199–206

[26] Kruskopf M and Elmquist R E 2018 Epitaxial graphene for quantum resistance metrology *Metrologia* **55** R27

[27] GIQS—Graphene impedance quantum standard—EMPIR 18SIB07

[28] Overney F, Flowers-Jacobs N E, Jeanneret B, Rüfenacht A, Fox A E, Underwood J M, Koffman A D and Benz S P 2016 Josephson-based full digital bridge for high-accuracy impedance comparisons *Metrologia* **53** 1045

[29] Bauer S, Behr R, Hagen T, Kieler O, Lee J, Palafox L and Schurr J 2017 A novel two-terminal-pair pulse-driven Josephson impedance bridge linking a 10 nF capacitance standard to the quantized Hall resistance *Metrologia* **54** 152

[30] Hagen T, Palafox L and Behr R 2017 A Josephson impedance bridge based on programmable Josephson voltage standards *IEEE Trans. Instrum. Meas.* **66** 1539–45

[31] Overney F, Flowers-Jacobs N E, Jeanneret B, Rufenacht A, Fox A E, Dresselhaus P D and Benz S 2020 Dual Josephson impedance bridge: towards a universal bridge for impedance metrology *Metrologia* **57** 065014

[32] Gournay P *et al* 2018 Comparison CCEM-K4.2017 of 10 pF and 100 pF capacitance standards *Metrologia* **56** 001

[33] Kozioł M, Kaczmarek J and Rybski R 2018 Characterization of PXI-based generators for impedance measurement setups *2018th Conf. Precis. Electromagn. Meas. (CPEM 2018)* (Paris, France) IEEE vol 7 pp 1–2 (https://ieeexplore.ieee.org/document/8500928)

[34] Ortolano M *et al* 2020 A comprehensive analysis of error sources in electronic fully-digital impedance bridges *IEEE Trans. Instrum. Meas.* (http://doi.org/10.1109/TIM.2020.3034115)

[35] Kaczmarek J, Rybski R and Kozioł M 2016 The polyphase ac voltage source for digital impedance bridges *Final Dissemination Workshop of EMRP Projects AIM QuTE, GraphOhm and Q-WAVE* (Prague, Czech Republic) p 5

[36] Ortolano M, Palafox L, Kučera J, Callegaro L, D'Elia V, Marzano M, Overney F and Gülmez G 2018 An international comparison of phase angle standards between the novel impedance bridges of CMI, INRIM and METAS *Metrologia* **55** 499

[37] Kampik M, Torarski J, Barwinek M M W, Rybski R, Kaczmarek J and Nissilä M K J 2015 Comparison of two buffers for impedance metrology *Meas. Autom. Monit.* **61** 127–31

[38] Symons P 2013 *Digital Waveform Generation* (Cambridge: Cambridge University Press)

[39] Callegaro L 2005 On strategies for automatic bridge balancing *IEEE Trans. Instrum. Meas.* **54** 529–32

[40] JCGM 102:2011 Evaluation of Measurement Data—Supplement 2 to the Guide to the Expression of Uncertainty in Measurement—Extension to Any Number of Output Quantities (BIPM)

[41] Zeier M, Hoffmann J and Wollensack M 2012 *Metas.UncLib*—a measurement uncertainty calculator for advanced problems *Metrologia* **49** 809

[42] Kambič *Air bath TK-190 US data sheet*

[43] Labs I *1404 Series Primary Standard Capacitor Datasheet*

[44] D'Elia V, Callegaro L, and Ortolano M 2018 Capacitance dependence versus atmospheric pressure of sealed-gas capacitors INRIM, TR 23/2018, May

[45] Delahaye F 1993 Series and parallel connection of multiterminal quantum Hall-effect devices *J. Appl. Phys.* **73** 7914–20

[46] Kibble B P and Rayner G H 1984 *Coaxial AC Bridges* (Bristol, UK: Adam Hilger Ltd)